physica status solidi a
www.pss-a.com

Doping-Dependent Phase Fractions in Hydrothermally Synthesized Mn-Doped $CuFeO_2$

*Nelson Igbinehi, Abdelfattah Mahmoud, Daniela Fenske, and Benedikt Klobes**

Using a simple hydrothermal method, $CuFe_{1-x}Mn_xO_2$ delafossite materials are produced and investigated by means of X-ray diffraction, ultraviolet–visible reflectance measurements, and electron microscopy. Up to nominally $x = 0.3$, the synthesis yields delafossite material, which generally consists of both the 2H and R3 phases without any impurities. Lattice parameters and the indirect optical bandgap of delafossite close to about 1.3 eV decrease upon increasing Mn content, which confirms the successful doping with Mn up to an actual Mn content of $x = 0.05$. The 2H phase fraction shows a pronounced and peaked dependence on Mn content with a maximum 2H mass fraction of about 27% at nominally $x = 0.01$, whereas the hexagonal particle morphology and the platelet size of about 500 nm as measured by both scanning and transmission electron microscopy are independent of the latter.

1. Introduction

The mineral $CuFeO_2$ is the archetype and eponym of the delafossite group. In general, these oxides exhibit the basic formula $A^IB^{III}O_2$, where A represents monovalent cations such as Cu, Ag, and Pd, and B represents trivalent metal ions as, e.g., Al, Fe, and Co. Depending on the stacking orientation of the double layers consisting of edge-sharing $B^{III}O_6$ octahedra and of triangularly arranged A^I layers, delafossite exists in a rhombohedral (R3) and hexagonal (2H) form with $R\bar{3}m$ and $P6_3/mmc$ space group, respectively.[1] $CuFeO_2$ is a semiconductor with an indirect optical bandgap at about 1.3 eV[2] and other favorable properties, which drive research into its application as an active anode material for lithium-ion and sodium-ion batteries,[3] for thermoelectric energy generation,[4,5] and as a catalyst for various catalytic approaches ranging from pollutant degradation to CO_2 conversion and solar energy conversion[6–9] among others. Besides, it is also of fundamental interest thanks to its magnetic properties and structures at low temperatures.[10,11]

Delafossite compounds in general and $CuFeO_2$, in particular, can be synthesized using various approaches, e.g., solid-state reactions,[12–14] sol–gel techniques,[3,15,16] and hydrothermal methods.[17–19] Solid-state reaction as well as sol–gel synthesis require high temperatures around 950 °C and, thus, are rather energy intensive in contrast to hydrothermal synthesis routes, which predominantly operate at temperatures well below 200 °C. Moreover, the high-temperature synthesis techniques usually yield a single R3 phase $CuFeO_2$, whereas the formation of both phases is a common, yet not fully understood observation in hydrothermally produced delafossite materials. Among the synthesis parameters known to affect 2H formation are reaction time, temperature, and basicity,[20] but doping effects on 2H and R3 fractions in $CuFeO_2$ are yet rather unexplored. However, as doping is very important for optimizing the applicability of $CuFeO_2$ and the phase mixture of hydrothermally synthesized delafossite can also impact the latter, we herein report on the 2H phase fraction upon doping $CuFeO_2$ with Mn. The respective samples were produced using a simple hydrothermal synthesis and were investigated using X-ray diffraction (XRD), ultraviolet–visible (UV–vis) spectroscopy, scanning electron microscopy (SEM), transmission electron microscopy (TEM), and energy dispersive X-ray analysis (EDX).

2. Results and Discussion

Using the hydrothermal synthesis described in Section 4, $CuFe_{1-x}Mn_xO_2$ could be successfully synthesized up to $x = 0.3$ as determined using XRD. Attempts to produce delafossite samples with $x > 0.3$ were unsuccessful, i.e., using an appropriate mixture of the reactants only a variety of oxides such as CuO, MnO, or Fe_2O_3 were formed. A representative XRD pattern obtained for $CuFe_{0.95}Mn_{0.05}O_2$ is shown in **Figure 1** and reveals

N. Igbinehi, B. Klobes
Hochschule Bremerhaven
Bremerhaven Institute of Nanotechnology
An der Karlstadt 8, 27568 Bremerhaven, Germany
E-mail: bklobes@hs-bremerhaven.de

A. Mahmoud
GREEnMat, UR CESAM
University of Liège
Allée du Six Août 13, B-4000 Liège, Belgium

D. Fenske
Fraunhofer Institute for Manufacturing Technology and Advanced Materials
Wiener Str. 12, 28 359 Bremen, Germany

The ORCID identification number(s) for the author(s) of this article can be found under https://doi.org/10.1002/pssa.202100713.

DOI: 10.1002/pssa.202100713

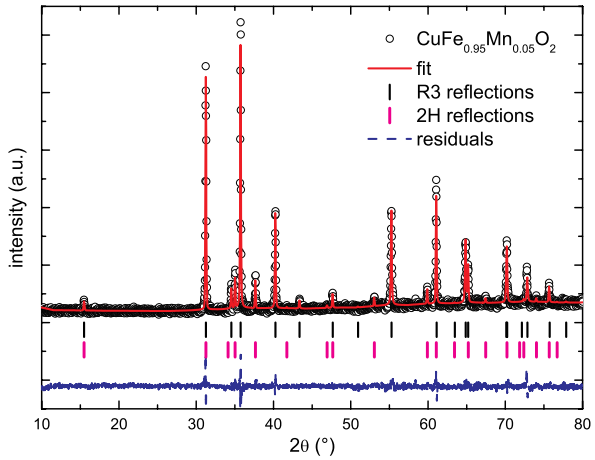

Figure 1. X-ray diffraction (XRD) pattern of the hydrothermally synthesized $CuFe_{1-x}Mn_xO_2$, in this case with $x = 0.05$. The tics represent XRD peaks due to the R3 and 2H phases, respectively. No impurity phases are present.

Table 1. Lattice constants a and c of the R3 and 2H phases in $CuFe_{1-x}Mn_xO_2$ determined by XRD. Above $x = 0.10$, no 2H phase could be detected. Additionally, the indirect bandgap $E_{g,ind}$ determined by UV–vis reflectance measurements and the relative Mn concentration c_{Mn} determined by EDX are listed.

x in $CuFe_{1-x}Mn_xO_2$	a [Å], R3	c [Å], R3	a [Å], 2H	c [Å], 2H	$E_{g,ind}$ [eV]	c_{Mn}
0	3.03619(4)	17.1621(4)	3.0357(2)	11.444(3)	1.38(1)	–
0.005	3.0362(2)	17.1627(4)	3.0358(3)	11.445(2)	1.38(1)	–
0.01	3.0356(1)	17.1672(1)	3.0354(2)	11.4429(8)	1.37(1)	0.0061
0.02	3.0352(1)	17.1675(8)	3.0351(1)	11.445(1)	1.34(1)	0.0122
0.05	3.0346(1)	17.1670(8)	3.0345(1)	11.4402(8)	1.33(3)	0.0264
0.10	3.0332(2)	17.158(1)	3.0331(2)	11.4366(9)	1.26(3)	0.0347
0.20	3.0336(5)	17.132(5)			1.30(2)	0.0533
0.30	3.0335(6)	17.135(4)			1.26(2)	0.0514

the two-phase nature of all samples consisting of both the 2H and R3 phases. No other phases were detected in any $CuFe_{1-x}Mn_xO_2$ samples. The fitted lattice parameters of both phases are summarized in **Table 1** and the calculated unit cell volume including the fitted 2H phase fractions are shown in **Figure 2**.

The lattice parameters determined for the undoped delafossite are in line with published values for both the R3[14,21,22] and the 2H phase.[23] Mn doping results in a decrease of lattice parameters and, consequently, of the unit cell volume of both phases (see Figure 2) up to a mangenese (Mn) content of $x = 0.1$. Above the latter value, samples are single R3 phase delafossite and the lattice parameters of the R3 phase stay constant. A similar decrease was reported for Mn-doped delafossite synthesized by solid-state reactions,[22,24] whereas other investigations based on the latter synthesis approach found only marginal changes upon Mn doping.[13,21] However, in combination with the bandgap presented in the following, the decrease of lattice parameters indicates that Mn is embedded in both phases. In contrast, the constancy above $x = 0.1$ likely reflects the stoichiometric limits achievable with the applied hydrothermal synthesis. A limited miscibility of $CuFeO_2$ and $CuMnO_2$, i.e., the limited substitution of Fe by Mn, is expected considering the structural difference of $CuMnO_2$ with monoclinic $C2/m$ space group to its $CuFeO_2$ counterpart. However, the nominal limit of about $x = 0.1$, which corresponds to an actual limit of $x = 0.05$ as discussed with respect to EDX measurements in the following, is significantly lower than miscibility/doping levels (of delafossite $CuFeO_2$) achieved using solid-state reactions with $x < 0.4$.[13]

Besides the constancy of R3 lattice parameters above a Mn content of 0.1, no 2H phase is formed in these samples and they solely consist of the R3 phase. Moreover, a strong dependency of the 2H phase fraction on the Mn content is observed (see Figure 2) with the maximal phase fraction of about 27% for $CuFe_{0.99}Mn_{0.01}O_2$. In general, the formation of both $CuFeO_2$ phases in doped and undoped samples is frequently observed following hydro- or solvothermal synthesis[19,25–27] under comparable basic conditions (2.2 mol L^{-1} NaOH in the presented case), whereas pure 2H formation requires very high basicity (more than 15 mol L^{-1} NaOH used by Jin and Chumanov[20]). Investigations of Ca-, Mg-, and Ni-doped and hydrothermally produced $CuFeO_2$[19,26,27] are compatible with the presented results on 2H fractions though the latter studies were limited either to relatively low or high doping levels. Xiong et al. observed no more 2H in Ca-doped delafossite at a doping level of 5%, which, however, was the lowest doping level studied except for the undoped compound. In contrast, Jiang et. al. reported an increase of the 2H phase fraction at low doping levels of Mg up to 0.5% with no higher dopant concentration. Additionally, in (3% and 6%) Ni-doped samples, a gradual decrease of the 2H fraction was published.[27] Thus, the peaked 2H phase fraction observed here for Mn doping complements and consolidates the previously mentioned studies. Based on the present data, the physicochemical reason for this behavior remains unclear. However, this might be caused by the bigger differences between the 2H and the $CuMnO_2$ structure than between 3R and crednerite. Certainly, basicity is not strongly enough affected by the addition of doping atom reactants to induce any change of phase fraction. Interestingly, the addition of an appropriate carbon source/carbon-based reactant might suppress 2H formation.[28,29]

The indirect optical bandgap $E_{g,ind}$ of the $CuFeO_2$ samples was determined using the approach proposed by Tauc et al.[30] and the quantity $F(R_\infty)$ (see Section 4) as a representative for the optical absorption coefficient. For pure $CuFeO_2$ and $CuFe_{0.8}Mn_{0.2}O_2$, the corresponding Tauc plots including the linear fits for determining $E_{g,ind}$ are shown in **Figure 3**. The bandgap values for all samples are summarized in Table 1 and decrease up to an Mn content of $x = 0.1$, beyond which $E_{g,ind}$ remains constant. Considering published experimental values ranging from 1.03 to 1.35 eV ,[2,8,27] ab initio calculations yielding 1.3 eV for the rhombohedral R3 phase,[31] and the bandgap of the pure 2H phase of 1.33 eV,[20] the bandgap of undoped $CuFeO_2$ $E_{g,ind} = 1.38(1)$ eV, determined here, is reasonable. The same applies for the observed decrease of $E_{g,ind}$ with increasing Mn content x, which both corroborates the successful doping in line with the decrease of lattice

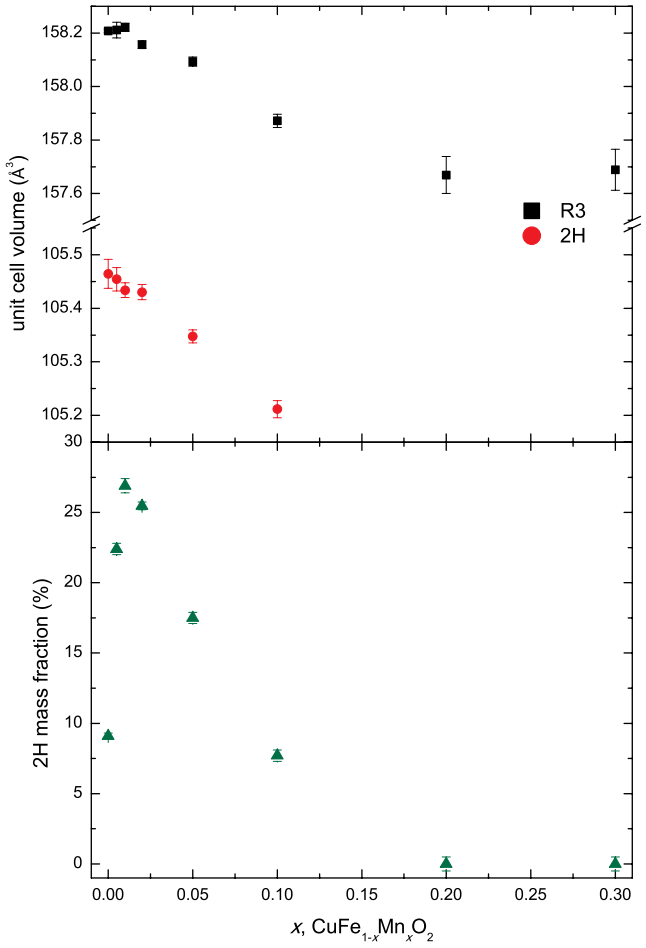

Figure 2. Unit cell volume of the R3 and 2H phases (top) and 2H mass fraction (bottom) of hydrothermally synthesized $CuFe_{1-x}Mn_xO_2$. For $x > 0.1$, no 2H phase was detected.

parameters as well as unit cell volume and agrees with a similar decrease observed in the case of Ni doping.[27] Due to the proximity of the bandgaps of the R3 and 2H phases however, any further analysis with respect to the impact of Mn doping on the phase-specific bandgaps is effectively prevented.

In contrast to its significant effect on phase fractions and the indirect bandgap, the Mn content had no observable effect on particle morphology. Representative images obtained by SEM and TEM are shown in **Figure 4**. In all cases, hexagonal platelets are formed with sizes ranging from about 500 to 800 nm, which is frequently observed for hydrothermally produced delafossite.[19,25,28] The Mn content was determined using EDX and is shown in Table 1. Thus, the actual Mn stoichiometry is about half of the nominal one resulting in an actual doping limit of 5%, which is obtained between 10% and 20% nominal doping (in line with the constancy of unit cell volume, see Figure 2). This is much lower than Mn levels obtained in samples synthesized by solid-state reactions[13,21] but comparable to hydrothermal results for Ni-doped delafossite.[27] Moreover, rather strong discrepancies between nominal and actual doping levels were also found for Mg- and Ca-doped $CuFeO_2$.[26,32] Two interesting questions result from these observations, which, however, cannot be comprehensively answered using the present data. First, there is the question concerning the apparent doping limit of about 5% and, second, the one concerning the difference between nominal and actual doping. One might speculate that the (actual) doping limit could be related to a reduced stability of $CuMnO_2$ in the hydrothermal environment as compared to $CuFeO_2$, but $CuMnO_2$ can be synthesized in similar ways compared to the procedure used here.[33] Notably, the doping limit agrees with the one reported to yield single-phase $CuFe_{1-x}Mn_xO_2$ using a solid-state reaction.[24] Another possibility could be the presumably complex defect structure of $CuFeO_2$ produced by hydrothermal synthesis which might not be able to accommodate further impurity/dopant atoms. Even if defects in delafossites, in

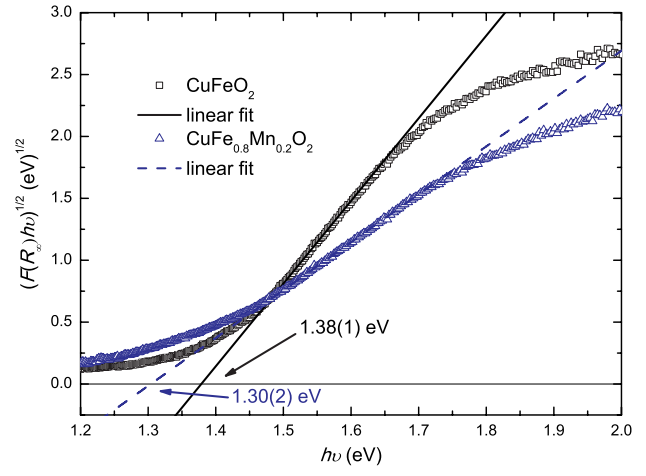

Figure 3. Tauc plot (see main text) based on the diffuse optical reflectance, represented by $F(R_\infty)$, of $CuFeO_2$ and $CuFe_{0.8}Mn_{0.2}O_2$ used to determine the indirect bandgaps, which are 1.38(1) and 1.30 eV(2), respectively.

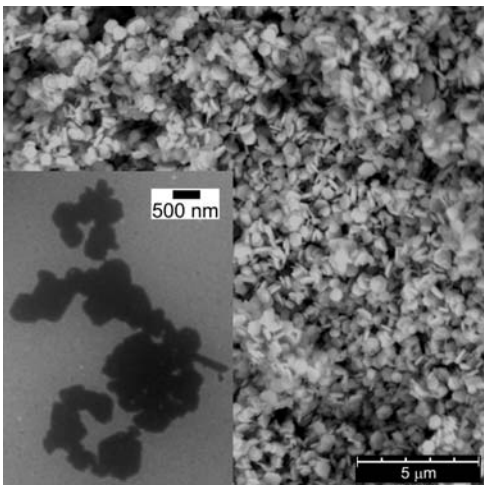

Figure 4. Representative scanning electron micrograph of $CuFe_{1-x}Mn_xO_2$ with $x = 0.05$ showing the typical hexagonal platelet morphology of the synthesized particles. The inset shows a transmission electron microscopy picture of the same sample after dilution. Electron microscopy images of other samples were almost identical.

general, and $CuFeO_2$, in particular, have not been extensively studied, it is known that antisite defects, interstitial oxygen, and vacancies are major contributors.[34–36] Besides, in a study on $CuAlO_2$ significant off-stoichiometries of all constituents were reported after hydrothermal synthesis.[34] The low formation energy of antisite defects, i.e., Cu on the Fe site, in $CuFeO_2$[35] might thus render those defects to be intrinsic antagonists to Mn doping. Additionally, the difference between nominal and actual doping levels might be related to the specific parameters of the co-precipitation process used.[37]

3. Conclusion

In summary, Mn-doped $CuFeO_2$ was produced using a hydrothermal route at moderate 160 °C up to nominally $CuFe_{0.9}Mn_{0.1}O_2$. Although the successful doping is reflected by a decrease of lattice parameters and a concomitant decrease of the indirect low-energy bandgap, the actual Mn content amounts to only half of the nominal concentration as determined by EDX measurements. Moreover, the actual Mn content is found to saturate at 5%. The powder particle shape of hexagonal platelets in the 500 nm range was found to be independent of the actual stoichiometry. However, the 2H phase fraction shows a pronounced dependence on the Mn doping level with a slight increase at very low Mn concentrations below 1% and a subsequent decrease and disappearance of the 2H phase. This offers the possibility to control delafossite phase fractions by appropriate doping levels and may find applications, e.g., in thermoelectric applications, in which phase boundaries can further limit the thermal conductivity and, thus, help to increase the thermoelectric figure of merit.

4. Experimental Section

Hydrothermal Synthesis of Mn-Doped $CuFeO_2$: Mn-doped $CuFeO_2$ samples were prepared by a hydrothermal method previously used for the synthesis of pure delafossite.[19,26] For undoped $CuFeO_2$, 7.5 mmol of both $CuSO_4 \times 5H_2O$ and $FeSO_4 \times 7H_2O$ as well as 110 mmol of NaOH were dissolved in 50 mL deionized water and magnetically stirred for 10 min. Afterward, the solution was poured into a 100 mL polytetrafluoroethylene (PTFE) lined autoclave and stored at 160 °C for 13 h. For $CuFe_{1-x}Mn_xO_2$, $MnSO_4 \times 4H_2O$ was added in appropriate amounts to the mixture before stirring and the amount of $FeSO_4 \times 7H_2O$ was reduced accordingly. The autoclave was allowed to cool down naturally to room temperature and, subsequently, the black product was washed two times using deionized water, once using ethanol, and subjected to centrifugation at about $5000 \times g$ for 5 min. The moist product/powder was eventually dried in air at 60 °C for 24 h.

Optical Reflectance Measurements: The UV–vis diffuse reflectance R_∞ of powder samples within the wavelength range from 250 to 1100 mm was measured using a UV–vis spectrometer (Avantes, AvaSpec-ULS2048CL) and a deuterium–halogen light source (Avantes, AVALIGHT-DHC). PTFE was used as a reflectance reference material. The optical absorption coefficient was estimated by the quantity $F(R_\infty)$ according to the Schuster–Kubelka–Munk formula $F(R_\infty) = (1 - R_\infty)^2/(2R_\infty)$.[38,39]

XRD: Crystal structure and phases of the Mn-doped $CuFeO_2$ powder samples were identified by XRD over the 2θ range from 10° to 80° with a Bruker D8 Discover Twin-Twin advance diffractometer using Cu K_α (doublet) radiation. Diffractograms were analyzed by Rietveld refinement using the software Jana2006.[40] The weighted profile R-factor, R_{wp}, ranged from 5.5 to 8.5% and the goodness of fit ranged between 1.3 and 1.9% in all cases.

SEM and EDX Analysis: A Phenom proX instrument placed in a glove box under inert conditions (Argon) was used for SEM and EDX measurements. The compact instrument has a four-quadrant backscatter electron detector. The EDX detector is an integrated silicon drift detector with Peltier cooling and an energy resolution of 140 eV.

TEM: TEM images were obtained using a benchtop low voltage TEM microscope (LVEM5, Delong America, Canada) operating at 5 kV. Powder samples were diluted in water, homogenized using ultrasound, and dropped onto Cu grids coated with thin carbon films for sample/particle support.

Acknowledgements

Open access funding enabled and organized by Projekt DEAL.

Conflict of Interest

The authors declare no conflict of interest.

Data Availability Statement

The data that support the findings of this study are available from the corresponding author upon reasonable request.

Keywords

$CuFeO_2$, delafossite, doping, XRD, 2H and R3 phases

Received: October 21, 2021
Revised: January 2, 2022
Published online:

[1] M. A. Marquardt, N. A. Ashmore, D. P. Cann, *Thin Solid Films* **2006**, *496*, 146.
[2] F. A. Benko, F. P. Koffyberg, *J. Phys. Chem. Solids* **1987**, *48*, 431.
[3] L. Lu, J.-Z. Wang, X.-B. Zhu, X.-W. Gao, H.-K. Liu, *J. Power Sources* **2011**, *196*, 7025.
[4] T. Nozaki, K. Hayashi, T. Kajitani, *J. Chem. Eng. Jpn.* **2007**, *40*, 1205.
[5] M. Tato, R. Shimonishi, M. Hagiwara, S. Fujihara, *ACS Appl. Energy Mater.* **2020**, *3*, 1979.
[6] C. Dai, X. Tian, Y. Nie, H.-M. Lin, C. Yang, B. Han, Y. Wang, *Environ. Sci. Technol.* **2018**, *52*, 6518.
[7] R. Wang, H. An, H. Zhang, X. Zhang, J. Feng, T. Wei, Y. Ren, *Appl. Surf. Sci.* **2019**, *484* 1118.
[8] Y.-H. Chang, H. Wang, T.-F. Siao, Y.-H. Lee, S.-Y. Bai, C.-W. Liao, J.-K. Zhuang, T.-W. Chiu, C.-H. Kuo, *J. Alloys Compd.* **2021**, *854* 157235.
[9] Q.-L. Liu, Z.-Y. Zhao, R.-D. Zhao, J.-H. Yi, *J. Alloys Compd.* **2020**, *819* 153032.
[10] N. Terada, S. Mitsuda, T. Fujii, D. Petitgrand, *J. Phys. Condens. Mater.* **2007**, *19*, 145241.
[11] B. Klobes, M. Herlitschke, K. Z. Rushchanskii, H.-C. Wille, T. T. A. Lummen, P. H. M. van Loosdrecht, A. A. Nugroho, R. P. Hermann, *Phys. Rev. B* **2015**, *92*, 1.
[12] E. Mugnier, A. Barnabé, P. Tailhades, *Solid State Ion.* **2006**, *177*, 607.
[13] T. Nozaki, K. Hayashi, T. Kajitani, *J. Electron. Mater.* **2010**, *39*, 1798.
[14] T. Elkhouni, M. Amami, C. V. Colin, A. B. Salah, *Mater. Res. Bull.* **2014**, *53* 151.
[15] R. F. Wu, W. Pan, S. Liu, J. Li, *Key Eng. Mater.* **2008**, *368–372* 663.
[16] Z. Deng, X. Fang, S. Wu, Y. Zhao, W. Dong, J. Shao, S. Wang, *J. Alloys Compd.* **2013**, *577* 658.

[17] X. Qiu, M. Liu, K. Sunada, M. Miyauchi, K. Hashimoto, *Chem. Commun.* **2012**, *48*, 7365.
[18] M. M. Moharam, M. M. Rashad, E. M. Elsayed, R. M. Abou-Shahba, *J. Mater. Sci. Mater. Electron.* **2014**, *25*, 1798.
[19] D. Xiong, Y. Qi, X. Li, X. Liu, H. Tao, W. Chen, X. Zhao, *RSC Adv.* **2015**, *5*, 49280.
[20] Y. Jin, G. Chumanov, *RSC Adv.* **2016**, *6*, 26392.
[21] K. Hayashi, R. Fukatsu, T. Nozaki, Y. Miyazaki, T. Kajitani, *Phys. Rev. B* **2013**, *87*, 064418.
[22] N. Barot, P. K. Mehta, A. Rao, R. Thomas, Y.-K. Kuo, S. K. Mishra, *J. Appl. Phys.* **2020**, *127*, 175704.
[23] H. Effenberger, *Acta Crystallogr. C* **1991**, *47*, 2644.
[24] F. Ye, H. Dai, K. Peng, T. Li, J. Chen, Z. Chen, N. Li, *J. Adv. Ceram.* **2020**, *9*, 444.
[25] Q. Xu, R. Li, C. Wang, D. Yuan, *J. Alloys Compd.* **2017**, *723* 441.
[26] T. Jiang, Y. Zhao, M. Liu, Y. Chen, Z. Xia, H. Xue, *Phys. Status Solidi A* **2018**, 215, *14* 1800056.
[27] Q. Deng, H. Chen, G. Wang, Y. Shen, F. Liu, S. Wang, *Ceram. Int.* **2020**, *46*, 598.
[28] N. Schmachtenberg, S. Silvestri, J. da Silveira Salla, G. L. Dotto, D. Hotza, S. L. Jahn, E. L. Foletto, *J. Environ. Chem. Eng.* **2019**, *7*, 102954.
[29] S. Xin, G. Liu, X. Ma, J. Gong, B. Ma, Q. Yan, Q. Chen, D. Ma, G. Zhang, M. Gao, Y. Xin, *Appl. Catal. B Environ.* **2021**, *280* 119386.
[30] J. Tauc, R. Grigorovici, A. Vancu, *Phys. Status Solidi B* **1966**, *15*, 627.
[31] K. P. Ong, K. Bai, P. Blaha, P. Wu, *Chem. Mater.* **2007**, *19*, 634.
[32] D. Xiong, Q. Zhang, S. K. Verma, X.-Q. Bao, H. Li, X. Zhao, *Mater. Res. Bull.* **2016**, *83* 141.
[33] X. Dong, J. Wang, J. Yang, X. Wang, L. Zhu, W. Zeng, J. Wang, F. Pan, *J. Electrochem. Soc.* **2021**, *168*, 100502.
[34] B. J. Ingram, G. B. González, T. O. Mason, D. Y. Shahriari, A. Barnabè, D. Ko, K. R. Poeppelmeier, *Chem. Mater.* **2004**, *16*, 5616.
[35] M. Ferri, J. Elliott, M. Farnesi Camellone, S. Fabris, S. Piccinin, *J. Phys. Chem. C* **2019**, *123*, 29589.
[36] M. Xu, Y. Sun, T. Li, B. Zhao, H. Dai, Z. Chen, *J. Asian Ceram. Soc.* **2021**, *9*, 699.
[37] K. Kurita, M. Yagisawa, R. Okazaki, *Jpn. J. Appl. Phys.* **2021**, *60*, 013001.
[38] A. Schuster, *Astrophys. J.* **1905**, *21* 1.
[39] P. Kubelka, F. Munk, *Z Techn. Physik.* **1931**, *12* 593.
[40] V. Petříček, M. Dušek, L. Palatinus, *Z. Kris. Cryst. Mater.* **2014**, *229*, 345.